V'yunov et al. Nanoscale Research Letters (2018) 13:98
https://doi.org/10.1186/s11671-018-2509-2

Nanoscale Research Letters

NANO EXPRESS Open Access

Impedance Analysis of Thin Films of Organic-Inorganic Perovskites $CH_3NH_3PbI_3$ with Control of Microstructure

Oleg V'yunov*, Anatolii Belous, Sofiia Kobylianska and Leonid Kovalenko

Abstract

The effect of starting reagents (PbI2:{CH_3NH_3I + CH_3NH_3Cl}) with different ratios in raw solutions on the microstructure of films of organic-inorganic perovskites $CH_3NH_3PbI_{3-x}Cl_x$, as well as on the electrical properties, has been investigated. It was found that the crystallinity is increased sharply when the ratio of the starting reagents increases from 1:1 to 1:2 and is changed slightly with a further increase of ratio to 1:3. It is shown that when the ratio of starting reagents varies, the morphology of the films changes; at a ratio of 1:1, the films consist of needle-like particles, and when the ratio is increased, particles become roundish and then faceted. Additionally, the average grain size is decreased. Complex impedance curves and I-V curves have been investigated for samples with different ratios of the starting reagents. With increasing this ratio, the concentration of charge carriers remains unchanged, the mobility of charge carriers decreases, and conductivity passes through a maximum at a ratio of 1:2. The electrical properties of film are the highest at the ratio of starting reagents 1:2 due to the effect of two competing factors: the growth of crystallinity and the decrease of grain size.

Keywords: Metal halide perovskite, Film, Microstructure, Complex impedance, I-V curve

PACS: 81.07.Pr, 81.07.–b, 84.37.+q, 72.40.+w

Background

The interest to hybrid organic-inorganic halides with perovskite structure has been increasing in recent years, which is due to successful attempts to increase the power conversion efficiency (PCE) into electrical energy in solar cells [1]. At the present time, in the halide system $APbX_3$ (A = CH_3NH_3, X = Cl, Br, I), a PCE of over 22% has been attained [2], which is higher of commercial monocrystalline silicon solar cells. The relatively easy [3] and low-cost production [4] of organic-inorganic hybrid perovskites should also be pointed out, which makes them promising for the creation of highly efficient and cheap solar cells. A considerable attention in the creation of solar cells is given to the problems of ultraviolet degradation and thermal decomposition [5]. The first problem is related to charge recombination at the interface between the electrode and perovskite, where structural defects act as recombination centers [6]. The formation of a large number of defects is caused by their low formation energy [7]. Simultaneous surface passivation of the perovskite/electrode interface and increasing the stability of the perovskite structure could increase the performance of solar cells. The structure imperfection can be reduced by the partial substitution of iodide ions with chlorine ions [8] or bromine ions [9]. At the same time, it was found that the grain boundaries do not enhance charge carrier recombination and can even facilitate charge separation processes [10, 11]. The ratio of the contributions of the grain interior and grain boundaries changes with grain size [12, 13]. Considerable changes in the microstructure of films are observed on changing stoichiometric ratio CH_3NH_3I:PbI_2 in initial solutions, which are used for the synthesis of organic-inorganic $CH_3NH_3PbI_3$ halides [14, 15]. The investigation of electrical characteristics (e.g., impedance spectroscopy) of the grain interior and grain boundaries

* Correspondence: vyunov@ionc.kiev.ua
Vernadsky Institute of General and Inorganic Chemistry of the National Academy of Sciences of Ukraine, Prospect Palladina, 32/34, Kiev 03142, Ukraine

of hybrid perovskites in solar cells is complicated because of the hysteresis effect [16]. This phenomenon is attributed to the accumulation of charge carriers at the interface between contacts. In this case, an inductive loop and negative capacitance at medium and low frequencies are being observed [17]. To reduce the influence of this effect, measurements can be made using planar electrodes. However, there are no data on the electrical characteristics of the grain interior and grain boundaries of perovskites (which differ significantly in the microstructure) determined by the complex impedance method using planar electrodes.

In this work, the effect of starting reagents ({CH_3NH_3I + CH_3NH_3Cl}:PbI_2) with different ratios in raw solutions on the microstructure of films of organic-inorganic perovskites $CH_3NH_3PbI_{3-x}Cl_x$, as well as on the electrical properties of grains and grain boundaries, has been investigated.

Methods

Methods of Synthesis

Lead iodide PbI_2, methylammonium chloride CH_3NH_3Cl (chemically pure), and pre-synthesized methylammonium iodide CH_3NH_3I [18] were used as starting reagents. Dried dimethylformamide (DMF, chemically pure) was used as the solvent.

For the deposition of $CH_3NH_3PbI_{3-x}Cl_x$ films, the starting reagents PbI_2, CH_3NH_3I, and CH_3NH_3Cl in stoichiometric ratios were dissolved in DMF and stirred at 70 °C for 1 h. Synthesis was carried out in a dry box. The resulting solution (room temperature) was applied to glass substrates by the spin-coating method. The rotation speed of the substrate was 40 rps. The thermal treatment of the films was carried out on the pre-heated hot plate in a temperature range of 70–150 °C for 30 min. The synthesis of organic-inorganic perovskites $CH_3NH_3PbI_{3-x}Cl_x$ was carried out at different ratios of the starting reagents PbI_2 and CH_3NH_3I (1:1, 1:2, 1:3).

Characterization

The phase composition was identified by X-ray powder diffractometry using a DRON-4-07 diffractometer (Cu$K\alpha$ radiation). The microstructure was studied using a microinterferometer MII-4 and a scanning electron microscope SEC miniSEM SNE 4500MB. The elemental composition of the films was studied using an EDAX Element PV6500/00 F spectrometer, which is included in the set of this microscope.

The electrical characteristics were investigated at alternating current at room temperature in the dark and with a change in the illumination up to 10 mW/cm^2 (corresponding to 0.1 of solar illuminance on a bright day), increasing the voltage from 0 to 40 V. Xe radiation from an Infolight H3 lamp (Akodgy, Seoul, South Korea) with a power of 50 W was used. The illumination was determined using a Lux/FC Light Meter DL-204. The complex impedance $Z = Z' + iZ''$ (where Z′ and Z″ are the real and imaginary parts of complex impedance) in a

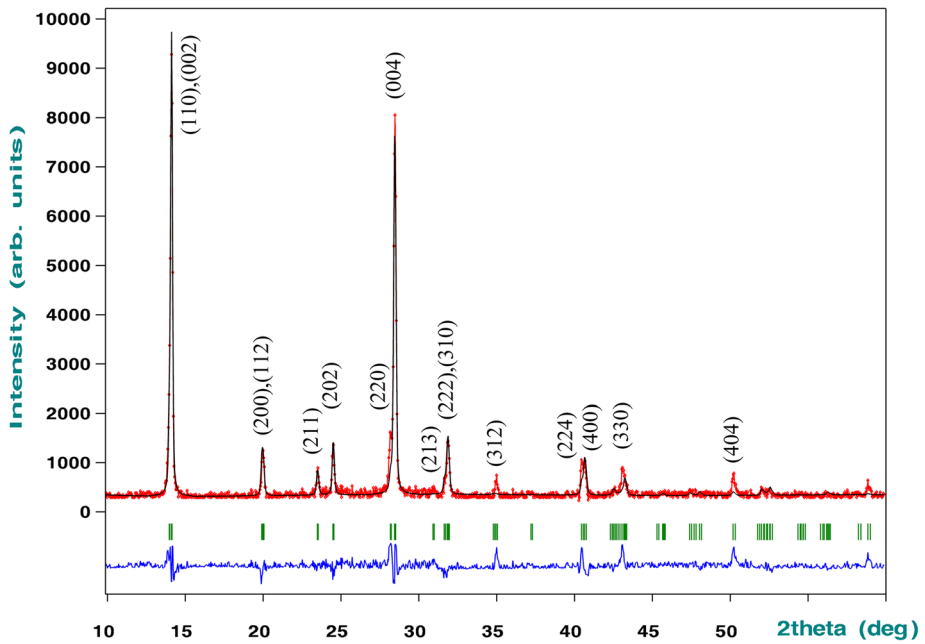

Fig. 1 Experimental (points) and calculated (lines) X-ray powder diffraction patterns of the $CH_3NH_3PbI_{2.98}Cl_{0.02}$ films after heat treatment at 80 °C and the ratio of starting reagents (PbI_2 and CH_3NH_3I) 1:2. Vertical bands indicate the positions of the peaks; the Miller indices are in parentheses. The difference curve is shown below

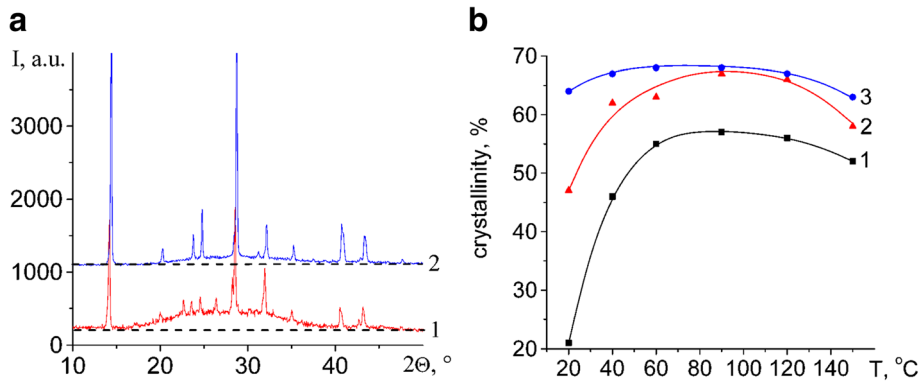

Fig. 2 **a** Comparison of XRD patterns of organic-inorganic films $CH_3NH_3PbI_{2.98}Cl_{0.02}$ synthesized at ratios of PbI_2 and CH_3NH_3I deposited at 20 °C (1) and 90 °C (2). **b** Film crystallinity as a function of deposition temperature of organic-inorganic films $CH_3NH_3PbI_{2.98}Cl_{0.02}$ synthesized at ratios of PbI_2 and CH_3NH_3I 1:1 (1), 1:2 (2), and 1:3 (3) (lines are drawn in for clarity)

wide frequency range (1 Hz–1 MHz) was determined using a 1260A Impedance/Gain-Phase Analyzer (Solartron Analytical). The equivalent circuit and the values of its components were determined using ZView® for Windows (Scribner Associates Inc., USA).

Results and Discussions

Organic-inorganic perovskites $CH_3NH_3PbI_{2.98}Cl_{0.02}$ were synthesized at different ratios of the starting reagents PbI_2 and CH_3NH_3I: PbI_2 + $0.98CH_3NH_3I$ + $0.02CH_3NH_3Cl$ (referred to as 1:1), PbI_2 + $1.98CH_3NH_3I$ + $0.02CH_3NH_3Cl$ (1:2), and PbI_2 + $2.98CH_3NH_3I$ + $0.02CH_3NH_3Cl$ (1:3); methylammonium iodide was partially substituted by 2, 1, and 0.67 mol% of CH_3NH_3Cl. At the ratio 1:1, the sample is single-phase after heat treatment at 80 °C but contains the PbI_2 phase at 150 °C, which is due to the decomposition of organic-inorganic perovskite. At the ratio 1:3, the sample contains remnants of additional phase at 80 °C, which are removed by heat treatment at 150 °C. At a ratio of 1:2, the sample is single-phase in a wide temperature range. The X-ray pattern of the sample corresponds to tetragonal symmetry (space group I4/mcm, No. 140) with the coordinates of atoms: Pb (4c) 0 0 0, I1 (8h) x y 0, I2 (4a) 0 0 ¼, C (16l) x y z, and N (16l) x y z [19]. Using the Rietveld full-profile analysis (Fig. 1), the unit cell parameters were refined (a = 0.8870(2) nm, c = 1.2669(8) nm, V = 0.9968(7) nm^3), which agrees with literature data [19].

The percent crystallinity for each film was estimated by the ratio of the area under each crystalline peak to the total area in the XRD spectra (Fig. 2a). Plots of the percent crystallinity as a function of deposition temperature of organic-inorganic films $CH_3NH_3PbI_{2.98}Cl_{0.02}$ synthesized at ratios of PbI_2 to CH_3NH_3I 1:1 (1), 1:2 (2), and 1:3 (3) are shown in Fig. 2b. The increasing temperature from room temperature to ~ 60 °C increases crystallinity. In the range of 60–120 °C, the crystallinity does not change significantly. A further increase in temperature decreases the crystallinity due to the disproportionation and PbI_2 separation. In the temperature range of 60–120 °C, the crystallinity is increased sharply with the ratio of the starting reagents from 1:1 to 1:2 (Fig. 2b, curves 1 and 2) and then is changed slightly (Fig. 2b, curves 2 and 3). Therefore, the crystallinity can significantly affect the properties of the films.

The elemental composition of the $CH_3NH_3PbI_{2.98}Cl_{0.02}$ films deposited from solutions with different ratios of the starting reagents PbI_2 and CH_3NH_3I (1:1, 1:2, and 1:3) was studied by the energy-dispersive X-ray spectroscopy (EDX) method (Fig. 3). The spectrum exhibits peaks of Ca, which is contained in the glass substrate [20]. It is seen from Fig. 2 that the intensity ratio of the Pb and I peaks is the same for the samples at different ratios of PbI_2 and CH_3NH_3I.

The shape and particle size of the obtained $CH_3NH_3PbI_{2.98}Cl_{0.02}$ films strongly depend largely on the stoichiometric ratio of the starting reagents. At the

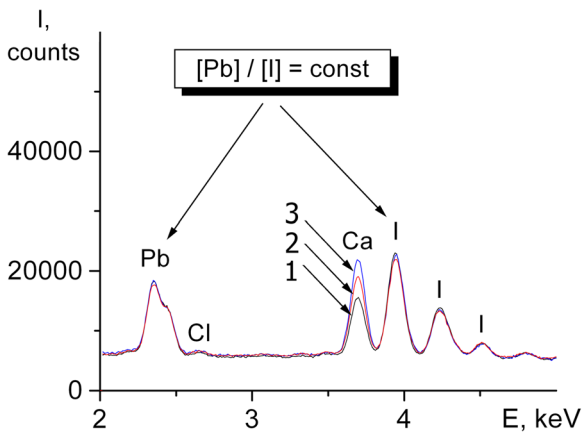

Fig. 3 EDX of $CH_3NH_3PbI_{2.98}Cl_{0.02}$ films after heat treatment at 80 °C and the ratio of starting reagents (PbI_2 and CH_3NH_3I) 1:1 (1), 1:2 (2), and 1:3 (3)

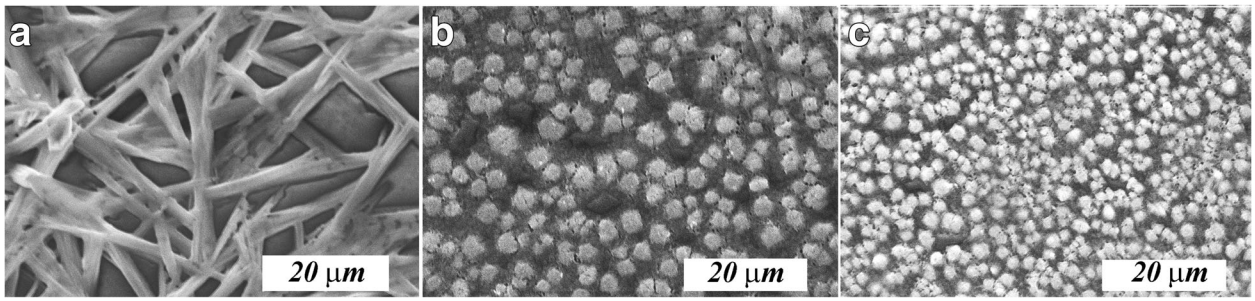

Fig. 4 Microstructure of films $CH_3NH_3PbI_{2.98}Cl_{0.02}$ after heat treatment at 80 °C and the ratio of starting reagents (PbI_2 and CH_3NH_3I) 1:1 (**a**), 1:2 (**b**), and 1:3 (**c**)

ratio PbI_2:CH_3NH_3I = 1:1, the films consist of needle-like particles, which are arranged along the substrate plane (Fig. 4). In the case of PbI_2:CH_3NH_3I = 1:2, roundish particles have been obtained (Fig. 4a). When the amount of methylammonium iodide is further increased (PbI_2:CH_3NH_3I = 1:3), a conversion from roundish particles to faceted particles is observed (Fig. 4b). In this case, the film thicknesses at different ratios of the starting reagents and at a heat treatment temperature of 80 °C are close together (900 nm).

The complex impedance data were collected on the day of synthesis, since the microstructure and properties of the samples may change during storage [21]. In the air atmosphere, a contribution of ionic conductivity appears, which manifests itself in the complex impedance spectra as an additional inclined line, which is characteristic of blocking electrodes [22, 23]. In order to avoid moisture and additional ionic conductivity, the measurements were made in a dry (humidity ≤ 7 ppm) nitrogen atmosphere [24]. For measurements, the film was deposited on a substrate with pre-applied electrodes (Fig. 5). The impedance curves of the multilayer system consist of organic-inorganic films deposited on glass substrate, which were measured in a dry atmosphere, are typical of materials characterized only by electronic conductivity (Fig. 6). The complex impedance diagram contains one semicircle in the medium frequency range (8 kHz–80 Hz), which can be described by an equivalent circuit consisting of a capacitor and resistor connected in parallel [25]. In the analysis, additional elements simulating the resistance of current-carrying parts and substrates were added; the parameters of which were determined by measuring the cell without deposited film.

The film parameters (dielectric constant and current density) were calculated using the partial capacitance method [26]. According to this approach, the measured multilayer system was represented as three simple planar capacitors with uniform filling and connected in parallel. For normal electric field components at the film interfaces, zero boundary conditions were assumed. The deposited film was conditionally divided into two parts (Fig. 5): the inner parallelepiped (width d and thickness h_2) and the outer parallelepiped (width l and thickness h_3). The capacity of the multilayer system (C) can be found as the sum of three partial capacitances $C = C_1 + C_2 + C_3$, where C_1, C_2, and C_3 are the capacitances of the parts of the planar capacitor, which are scattering fields in (1) the substrate, (2) the inner parallelepiped of the film, and (3) the outer parallelepiped of the film. The capacitance of the inner part of the film (part 2) is determined by the usual equation of a flat capacitor, $C_2 = \frac{\varepsilon\varepsilon_0(w\times h_2)}{d}$. The capacity of the substrate (part 1), as well as the capacity of the outer part of the film (part 3), was determined using the Schwarz-Christoffel conformal mapping transformation adapted by Gevorgian [27]. According to this method, the ellipse of electric fields in the sample is conditionally transformed into a rectangle. In this case, the capacitance of the substrate will be expressed by the formulas $C_1 = \frac{\varepsilon\varepsilon_0 K(k')}{2K(k)}$ and $k' = \sqrt{1-k^2}$, where K (k) is a complete elliptic integral of the first kind; k is the modulus of the elliptic integral; ε_0 is the permittivity of free space; and ε_r is the relative permittivity of the substrate. Glass of E class (radio engineering) with low dielectric loss and $\varepsilon = 6.6$ was used as the substrate [28]. To

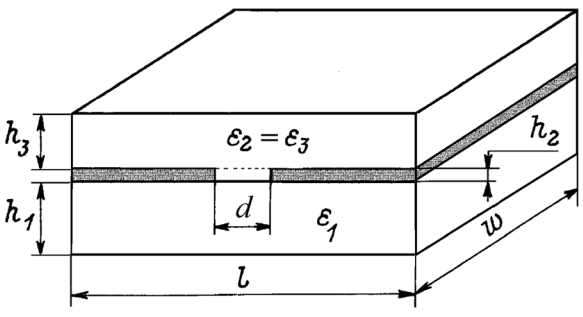

Fig. 5 The scheme of the measured multilayer system consisting of a substrate (l = 16 mm, w = 24 mm, h_1 = 1 mm), on which electrodes of thickness h_2 = 90 nm were deposited at a distance d = 250 μm, and the film under investigation was h_3 = 500 nm thick

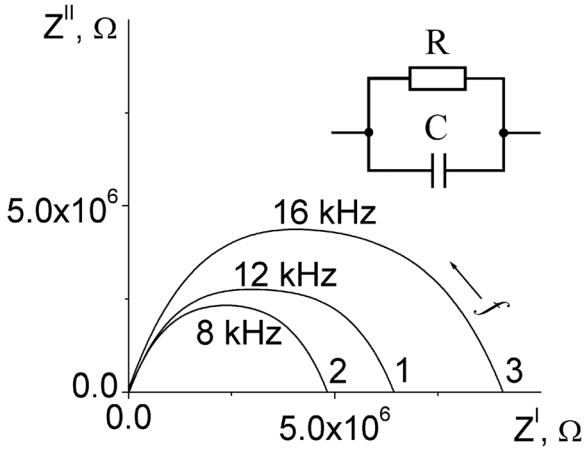

Fig. 6 Complex impedance diagrams (Nyquist plots) and equivalent circuit of multilayer system consists of perovskite organic-inorganic films prepared at the ratio of starting reagents (PbI_2 and CH_3NH_3I) 1:1 (1), 1:2 (2), and 1:3 (3) on glass substrate at an illumination of 30 klx. Measurements performed at a voltage of 1 V in a dry atmosphere. The numbers above the curves are the frequency (Hz)

solve elliptic integrals, we used the approximation proposed in [29]. Using a similar formula, the capacity of the outer part of the film was calculated. The experimental permittivity $\varepsilon = 52$ was determined, and this value is in agreement with the published data. The calculations based on density functional theory and density functional perturbation theory showed that the optical contribution to permittivity is $\varepsilon_\infty = 5.6–6.5$, and the dielectric contribution is $\varepsilon_0 = 18.0–37.3$ for the low-temperature cubic phase (Pm-3 m) [30]. Direct measurements yielded $\varepsilon \sim 15–18$ for low-temperature cubic phase (Pm-3 m) and $\varepsilon \sim 60$ for the room temperature tetragonal phase (I4/mcm) [31].

Figure 7 shows the current density calculated from impedance data vs voltage applied to organic-inorganic films. The dark current is linearly dependent on the applied voltage, while under illumination, several linear regions are observed (Fig. 7). Previously, three regions were observed on the I-V curve of a single-crystal organic-inorganic perovskite, which were described as a change from the ohmic region to the trap-filled limit (TFL) region, and further to the Child region [32]. These regions can be observed at voltages of tens of volt per millimeters (depending on the sample and the type of electrode) and can be used to calculate the characteristics of charge carriers (namely, density and mobility) [33]. In particular, the dependence of current (I) on electric field (V) in the Child region is described by the equation $j = (9/8)\varepsilon\mu V^2/d^3$ (where ε is the permittivity of the sample, μ is the mobility of charge carriers, d is the distance between the electrodes), which makes it possible to determine the mobility of charge carriers. In the ohmic region, the current-voltage dependence is described by the equation $j = e\mu nV/d$ (where n is the density of charge carriers). Using the previously calculated mobility (in the Child region) of charge carriers, the density of charge carriers can be determined.

The Child law describes the current flow limited by a space charge in the mobility mode (trap-free quadratic relation) and is observed in dielectric materials that contain no traps [34]. When a relatively low voltage is applied to an unilluminated film, the density of injected carriers is small relative to the density of traps. So current-voltage curve in the investigated range of voltages obeys the linear Ohm's law (Fig. 7a, curve 1). Under high illumination, photo-generated carriers deactivate the trapping defects, and at a sufficiently high voltage, a

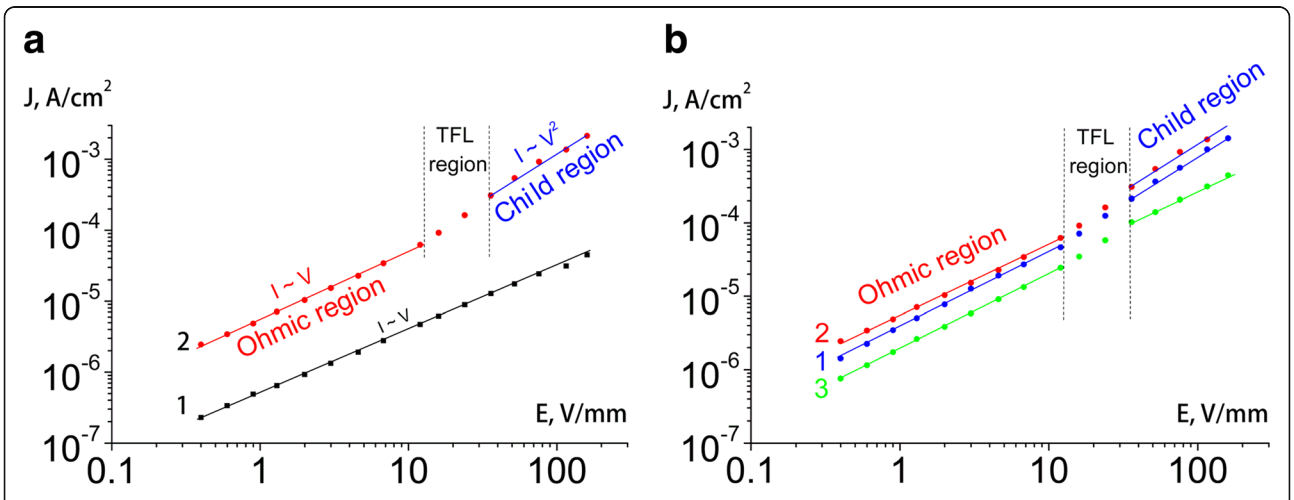

Fig. 7 Dependence of the current density on the voltage of **a** the organic-inorganic prepared at the ratio of starting reagents (PbI_2 and CH_3NH_3I) 1:2 at different illumination levels, 0 (1) and 30 klx (2), and **b** the organic-inorganic film prepared at the ratio of starting reagents 1:1 (1), 1:2 (2), and 1:3 (3) at an illumination of 30 klx

trap-free mobility mode is observed, and the dependence obeys the quadratic Child law (Fig. 7, curve 2) [35].

As can be seen from Fig. 7b, the organic-inorganic film obtained with a ratio of the starting reagents of 1:2 has the maximum conductivity among the samples investigated. In addition, an increase in the ratio of the starting reagents results in a decrease in charge carrier mobility. The decrease in the slope of the plot in the Child region confirms this fact. The same slope in the ohmic region at the same level of illumination indicates a close amount of charge carriers generated.

Conclusions

It has been shown that when the ratio of the starting reagents (PbI_2:CH_3NH_3I) is changed, the crystallinity and morphology of films changes. In particular, the crystallinity is increased sharply when the ratio of the starting reagents increases from 1:1 to 1:2 and is changed slightly with a further increase of ratio to 1:3. At the ratio of the starting reactants 1:1, the films consist of needle-like particles, which are arranged along the substrate plane. When the methylammonium iodide content is increased, a conversion to roundish and then to faceted particles is observed. Additionally, the average grain size is decreased. Inclined lines on the complex impedance plots of samples measured in the air atmosphere (humidity ~ 65%) are associated with the appearance of ionic conductivity in a liquid dielectric. In the case of measurements in a dry atmosphere, three regions were observed on the I-V curve obeying Ohm's law, the trap-filled limit, and the Child law. With an increase in the ratio of the starting reagents, the mobility of the charge carriers decreases, and the conductivity passes through a maximum at a ratio of 1:2. At the same level of illumination, the same number of charge carriers was generated. The electrical properties of the film are highest at the ratio of starting reagents 1:2 due to the effect of two competing factors: the growth of crystallinity and the decrease of grain size.

Abbreviations

CPE: Constant phase element; DC: Direct current; DMF: Dimethylformamide, C_3H_7NO; EDX: Energy-dispersive X-ray spectroscopy; I-V curves: Current-voltage curve; PCE: Power conversion efficiency; SEM: Scanning electron microscopy; XRD: X-ray diffraction

Acknowledgements

The work was carried out with the financial support from the targeted research program of the Ukrainian National Academy of Sciences "Fundamental Issues of Creation of Novel Nanomaterials and Nanotechnologies" (Novel Nanomaterials).

Authors' contributions

AG supervised the work and finalized the manuscript. OV performed the X-ray powder diffraction, SEM, and EDX investigations and took part in analyzing the obtained results. SK synthesized the films of hybrid organic-inorganic halides with perovskite structure. KL collected the data of complex impedance and fitted these data using equivalent circuits. AG, OV, and SK contributed on the drafting and revision of the manuscript. All authors read and approved the final manuscript.

Competing Interest

The authors declare that they have no competing interests.

Publisher's Note

Received: 27 December 2017 Accepted: 2 April 2018
Published online: 12 April 2018

References

1. Brenner TM, Egger DA, Kronik L, Hodes G, Cahen D (2016) Hybrid organic–inorganic perovskites: low-cost semiconductors with intriguing charge-transport properties. Nat Rev Mater 1:15007
2. Yang WS, Park B-W, Jung EH, Jeon NJ, Kim YC, Lee DU et al (2017) Iodide management in formamidinium-lead-halide–based perovskite layers for efficient solar cells. Science 356(6345):1376–1379
3. Kim H-S, Im SH, Park N-G (2014) Organolead halide perovskite: new horizons in solar cell research. J Phys Chem C 118(11):5615–5625
4. Cahen D, Lubomirsky I (2017) Self-repairing energy materials: sine qua non for a sustainable future. Acc Chem Res 50(3):573–576
5. Zhang P, Wu J, Wang Y, Sarvari H, Liu D, Chen ZD et al (2017) Enhanced efficiency and environmental stability of planar perovskite solar cells by suppressing photocatalytic decomposition. J Mater Chem A 5(33):17368–17378
6. Buin A, Comin R, Xu J, Ip AH, Sargent EH (2015) Halide-dependent electronic structure of organolead perovskite materials. Chem Mater 27(12):4405–4412
7. Buin A, Pietsch P, Xu J, Voznyy O, Ip AH, Comin R et al (2014) Materials processing routes to trap-free halide perovskites. Nano Lett 14(11):6281–6286
8. Berhe TA, Su W-N, Chen C-H, Pan C-J, Cheng J-H, Chen H-M et al (2016) Organometal halide perovskite solar cells: degradation and stability. Energy Environ Sci 9(2):323–356
9. Jeon NJ, Noh JH, Yang WS, Kim YC, Ryu S, Seo J et al (2015) Compositional engineering of perovskite materials for high-performance solar cells. Nature 517(7535):476–480
10. Edri E, Kirmayer S, Mukhopadhyay S, Gartsman K, Hodes G, Cahen D (2014) Elucidating the charge carrier separation and working mechanism of $CH_3NH_3PbI_{3-x}Cl_x$ perovskite solar cells. Nat Commun 5:3461
11. Yun JS, Ho-Baillie A, Huang S, Woo SH, Heo Y, Seidel J et al (2015) Benefit of grain boundaries in organic–inorganic halide planar perovskite solar cells. J Phys Chem Lett 6(5):875–880
12. Li S, Zhang P, Chen H, Wang Y, Liu D, Wu J et al (2017) Mesoporous PbI_2 assisted growth of large perovskite grains for efficient perovskite solar cells based on ZnO nanorods. J Power Sources 342:990–997
13. Wang Y, Wu J, Zhang P, Liu D, Zhang T, Ji L et al (2017) Stitching triple cation perovskite by a mixed anti-solvent process for high performance perovskite solar cells. Nano Energy 39:616–625
14. Manser JS, Reid B, Kamat PV (2015) Evolution of organic–inorganic lead halide perovskite from solid-state iodoplumbate complexes. J Phys Chem C 119(30):17065–17073
15. Belous AG, V'yunov OI, Kobylyanskaya SD, Ishchenko AA, Kulinich AV (2018) Influence of synthesis conditions on the morphology and spectral-luminescent properties of films of organic-inorganic perovskite $CH_3NH_3PbI_{2.98}Cl_{0.02}$. Russ J Gen Chem 88(1):114–119
16. Meloni S, Moehl T, Tress W, Franckevičius M, Saliba M, Lee YH et al (2016) Ionic polarization-induced current–voltage hysteresis in $CH_3NH_3PbX_3$ perovskite solar cells. Nat Commun 7:10334
17. Fabregat-Santiago F, Kulbak M, Zohar A, Vallés-Pelarda M, Hodes G, Cahen D et al (2017) Deleterious effect of negative capacitance on the performance of halide perovskite solar cells. ACS Energy Letters 2(9):2007–2013
18. Qiu J, Qiu Y, Yan K, Zhong M, Mu C, Yan H et al (2013) All-solid-state hybrid solar cells based on a new organometal halide perovskite sensitizer and one-dimensional TiO_2 nanowire arrays. Nano 5(8):3245–3248
19. Kawamura Y, Mashiyama H, Hasebe K (2002) Structural study on cubic–tetragonal transition of $CH_3NH_3PbI_3$. J Phys Soc Jpn 71(7):1694–1697
20. Barbieri L, Ferrari AM, Lancellotti I, Leonelli C, Rincón JM, Romero M (2000) Crystallization of (Na_2O–MgO)–CaO–Al_2O_3–SiO_2 glassy systems formulated from waste products. J Amer Ceram Soc 83(10):2515–2520
21. Huang W, Manser JS, Kamat PV, Ptasinska S (2015) Evolution of chemical composition, morphology, and photovoltaic efficiency of $CH_3NH_3PbI_3$ perovskite under ambient conditions. Chem Mater 28(1):303–311

22. Christians JA, Fung RC, Kamat PV (2013) An inorganic hole conductor for organo-lead halide perovskite solar cells. Improved hole conductivity with copper iodide. J Am Chem Soc 136(2):758–764
23. Schmidt W (1982) Elementary processes in the development of the electrical breakdown of liquids. IEEE Trans Electr Insul 6:478–483
24. High pure nitrogen, Linde Gas, Dnieper, Ukraine, corresponds to ISO 2435: 1973 Nitrogen for use in aircraft (https://www.iso.org/standard/7345.html) and DSTU 9293:2009 (http://shop.uas.org.ua/ua/azot-gazoobraznyj-i-zhidkij-tehnicheskie-uslovija.html). Accessed 6 Apr 2018.
25. Dualeh A, Moehl T, Tétreault N, Teuscher J, Gao P, Nazeeruddin MK et al (2013) Impedance spectroscopic analysis of lead iodide perovskite-sensitized solid-state solar cells. ACS Nano 8(1):362–373
26. Vendik OG, Zubko SP, Nikol'skii MA (1999) Modeling and calculation of the capacitance of a planar capacitor containing a ferroelectric thin film. Tech Phys 44(4):349–355
27. Gevorgian SS, Martinsson T, Linner PL, Kollberg EL (1996) CAD models for multilayered substrate interdigital capacitors. IEEE Trans Microw Theory Tech 44(6):896–904
28. Kolesov YI, Kudryavtsev MY, Mikhailenko NY (2001) Types and compositions of glass for production of continuous glass fiber. Glas Ceram 58(5):197–202
29. den Otter MW (2002) Approximate expressions for the capacitance and electrostatic potential of interdigitated electrodes. Sensors Actuators A Phys 96(2):140–144
30. Brivio F, Walker AB, Walsh A (2013) Structural and electronic properties of hybrid perovskites for high-efficiency thin-film photovoltaics from first-principles. Apl Mater 1(4):042111
31. Onoda-Yamamuro N, Matsuo T, Suga H (1992) Dielectric study of $CH_3NH_3PbX_3$ (X = Cl, Br, I). J Phys Chem Solids 53(7):935–939
32. Adinolfi V, Yuan M, Comin R, Thibau ES, Shi D, Saidaminov MI et al (2016) The in-gap electronic state spectrum of methylammonium lead iodide single-crystal perovskites. Adv Mater 28(17):3406–3410
33. Peng W, Miao X, Adinolfi V, Alarousu E, El Tall O, Emwas A-H et al (2016) Engineering of $CH_3NH_3PbI_3$ perovskite crystals by alloying large organic cations for enhanced thermal stability and transport properties. Angew Chem Int Ed 55(36):10686–10690
34. Child CD (1911) Discharge from hot CaO. Phys Rev (Series I) 32(5):492
35. Rose A (1955) Space-charge-limited currents in solids. Phys Rev 97(6):1538